Letters

A Simple Phase-Shift Modulation Using Parabolic Carrier for Dual Active Bridge DC–DC Converter

Yunting Liu, *Member, IEEE*, Xiaorui Wang, *Member, IEEE*, Wei Qian, Ameer Janabi, *Member, IEEE*, Bingsen Wang, *Senior Member, IEEE*, Xi Lu, Ke Zou, Chingchi Chen, and Fang Z. Peng, *Fellow, IEEE*

***Abstract*—The power transfer of a dual active bridge (DAB) dc–dc converter is not linearly proportional to the phase shift between the two active bridges. When the DAB converter controller receives the power reference, the phase shift needs to be obtained by either solving a quadratic equation online or looking up from a table. The online calculation method is computationally inefficient. The lookup table method has only limited operating points. In addition, when using interpolation to find missing operating points from the table, the control accuracy will be reduced. This letter proposes a simple phase-shift modulation using a parabolic carrier. The proposed method converts the power command into phase shift by modulation. Therefore, the solving of the quadratic equation can be eliminated. The Verilog results are provided to verify the proposed parabolic carrier. A case study of DAB with sinusoidal ripple current charging concept is provided to demonstrate the advantage of the proposed method.**

***Index Terms*—Digital control, dual active bridge (DAB), parabolic carrier, PWM modulation.**

I. Introduction

A DUAL active bridge (DAB) topology is shown in Fig. 1. This topology is widely used in electric vehicle (EV) on-board charger applications [1]. The DAB control algorithms normally include at least one calculation of square root since the power transfer of DAB is not linearly proportional to the phase shift. The calculation of square root consumes many computing resources in a digital signal processor (DSP) since it requires several iterations to achieve acceptable accuracy [2]. This makes it difficult for current DSPs to calculate multiple square roots in one switching cycle [3].

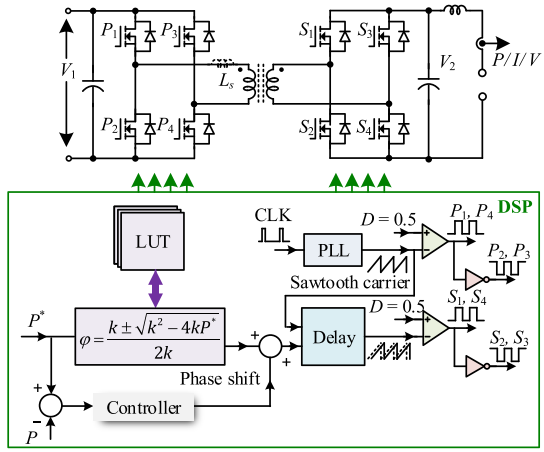

Fig. 1. Typical DAB with PWM-embedded DSP.

To reduce the computational burden of the DSP, lookup tables (LUTs) and linear interpolation are often used instead of online calculations. Small LUT can cause inaccurate control since interpolation is a linear approximation, whereas large LUTs consume a lot of DSP memory.

The one-cycle control (OCC) [4] introduces a nonlinear carrier concept to power converters. The OCC demonstrates a fast response to dynamic changes. Based on the OCC, Zhang [5] proposed a parabolic current control for voltage source inverter. The authors in [4] and [5] focused on creating feedback control with nonlinear carriers other than using the nonlinear carriers to reduce computational burden. In most cases, they are using an external high-speed high-precision DAC [6] or using an architecture of analog amplifiers [7] to implement the nonlinear carrier. The drawback of [6] is that a DAC with both high speed and high precision is required to generate precise parabolic carriers with minimized propagation delay. The DAC is replaced with operational-amplifier-based integrators and summators as the parabolic carrier generator in [7]. Additional analog switches are required to reset the parabolic carriers. Since high precision

Manuscript received December 1, 2019; revised January 3, 2020; accepted January 5, 2020. Date of publication January 13, 2020; date of current version April 22, 2020. This letter was presented in part at the 7th Workshop on Wide Bandgap Power Devices and Applications, Raleigh, NC, USA, 2019 [8]. *(Corresponding author: Yunting Liu.)*

Y. Liu is with the Department of Electrical Engineering and Computer Science, the University of Tennessee, Knoxville, TN 37996 USA (e-mail: yliu193@utk.edu).

X. Wang is with the Thermo King Corporation, Minneapolis, MN 55420 USA (e-mail: wangx110@msu.edu).

W. Qian, A. Janabi, and B. Wang are with the Michigan State University, Lansing, MI 48824 USA (e-mail: qianwei@msu.edu; janabiam@egr.msu.edu; bingsen@egr.msu.edu).

X. Lu, K. Zou, and C. Chen are with the Ford Motor Company, Dearborn, MI 48121 USA (e-mail: xlu24@ford.com; kzou2@ford.com; cchen4@ford.com).

F. Z. Peng is with the Center for Advanced Power Systems, Florida State University, Tallahassee, FL 32310 USA (e-mail: peng@caps.fsu.edu).

Color versions of one or more of the figures in this article are available online at https://ieeexplore.ieee.org.

Digital Object Identifier 10.1109/TPEL.2020.2966537

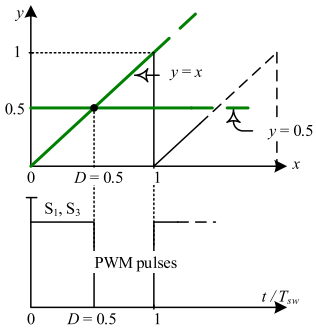

Fig. 2. Comparator converts digital signal into analog signal.

of the parabolic carrier is required to ensure the control performance, operational amplifiers with very small input offset current are preferred. Furthermore, a precise voltage reference chip is required to generate the input voltage of the parabolic carrier generator. These precise analog components would increase the cost of the control system.

This letter proposes a simple phase-shift modulation method using the parabolic carrier for DAB converters to remove the square root computation from control algorithms. This letter is organized as follows. The derivation of the parabolic carrier is presented in Section II. The implementation of the parabolic carrier is provided in Section III. Section IV evaluates the advantages of this method in terms of computational efficiency. The Verilog implementation of the parabolic carrier is provided in Section V. A DAB converter with sinusoidal-ripple-current (SRC) charging concept is studied to demonstrate the effectiveness of the proposed method in Section V.

II. Derivation of Parabolic Carrier

A typical DAB with DSP is shown in Fig. 1. When the DSP receives a power reference P^*, this piece of information will be used in both feedback and feed-forward loop. In the feedback loop, the output power of DAB is measured and compared with the power reference P^*. The error will then be sent to a controller to generate a phase shift to compensate the power mismatch. In the feed-forward loop, the DSP will either calculate the corresponding phase shift online or use LUT. The sum of the feedback loop and the feed-forward loop becomes the final phase shift command. The DSP then generates a sawtooth carrier with the phase shift for the secondary side H-bridge (S_1–S_4). The sawtooth carrier is compared with a fixed duty cycle $D = 0.5$ to generate the gating signal for the DAB under single phase shift (SPS) control.

Notice that the role of the comparator is to convert the digital signal $D = 0.5$ into an analog signal. Fig. 2 shows how the comparator converts the digital signal into an analog signal.

As shown in Fig. 2, the comparator is to convert the digital signal into analog signal by graphically solving an equation set

$$\begin{cases} y = 0.5 \\ y = x. \end{cases} \tag{1}$$

The intersection of $y = 0.5$ and $y = x$ is the solution of (1), which is $x = 0.5$. This indicates that pulsewidth modulation

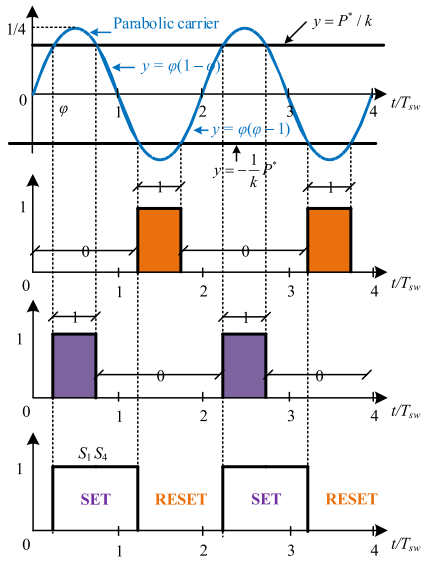

Fig. 3. Resulting gating signal of parabolic carrier based DAB.

(PWM) is equivalent to graphically solving an equation. Although this simple example does not help much in reducing the computation, this concept can be extended into more complicated calculations.

The most complicated calculation in DAB is to derive the phase shift from the power command. For example, the output power of DAB with SPS control is [9]

$$P = \frac{nV_1V_2}{2f_sL_s}\varphi(1-\varphi) \tag{2}$$

where n is the turns ratio of the transformer, V_1 is the primary side dc voltage, V_2 is the secondary side dc voltage, f_s is the switching frequency, L_s is the leakage inductance of the transformer, and φ is the phase shift. The corresponding phase shift φ as a function of P^* is as follows:

$$\varphi = \frac{k \pm \sqrt{k^2 - 4kP^*}}{2k} \tag{3}$$

where $k = nV_1V_2/(2f_sL_s)$. In order to find the solution to (2), one can solve it graphically. Decompose (2) into an equation set as follows:

$$\begin{cases} y = P^*/k \\ y = \varphi(1-\varphi). \end{cases} \tag{4}$$

As shown in Fig. 3, the intersection of $y = P^*/k$ and $y = \varphi(1-\varphi)$ is the solution of (4). The carrier becomes the combination of $y = \varphi(1-\varphi)$ and $y = \varphi(\varphi-1)$. $y = P^*/k$ and $y = -P^*/k$ are the reference. $y = \varphi(1-\varphi)$ and $y = P^*/k$ determine the secondary side voltage rising edge. $y = \varphi(\varphi-1)$ and $y = -P^*/k$ determine the secondary side voltage falling edge. Therefore, the square root calculation can be removed from control algorithms.

III. Implementation of Parabolic Carrier

The parabolic carrier can be implemented by using digital counters, shifters, and adders. These three elements are basic blocks in digital circuits such as complex programmable logic

device (CPLD), field-programmable gate array (FPGA), and many other controller chips. The commonly used DSPs are not suitable to test the proposed concept. The manufacturers of those controller chips may prohibit the reconfiguration of the microcontroller's hardware resources. The value of the proposed implementation of parabolic carrier is to provide a potential way to upgrade the counter-based PWM microcontroller units (MCUs) such as TI MCUs with relatively low cost.

Note that the carrier $y = \varphi(1-\varphi) = \varphi - \varphi^2 = \int 1 d\varphi - 2\int \varphi d\varphi$. $\int 1 d\varphi$ can be implemented by a counter. $\int \varphi d\varphi$ can be implemented by accumulating the counter value in an adder. Since the integral is implemented in a digital circuit, the output of adder needs to be scaled down by a shift block.

The targeting switching frequency is $f_{\rm sw}$. The digital circuit system clock frequency is set to be

$$f_{\rm sys} = 2^k \cdot f_{\rm sw} \tag{5}$$

where k is a positive integer. The system clock is set to 2^k times of switching frequency because it can simplify the rescale of the register value by using shift command later. 2^k should be at least 100 to secure necessary resolution for the PWM pulses. The counter register value is

$$\text{Counter}_{t_n} = \sum_{j=2^k\cdot\lfloor n/2^k \rfloor}^{n} j-(j-1) \forall t_n \tag{6}$$

where $\lfloor \bullet \rfloor$ denotes the floor operation. t_n is the system clock. Define $\tau_n = 2^k \cdot \lfloor n/2^k \rfloor$. Equation (6) can be rewritten as follows:

$$\text{Counter}_{t_n} = \sum_{j=\tau_n}^{n} f_{\rm sys} \cdot (t_j - t_{j-1}) = 2^k \cdot \sum_{j=\tau_n}^{n} f_{\rm sw} \cdot (t_j - t_{j-1}) \tag{7}$$

$$\text{Counter}_{t_n} = 2^k \cdot \sum_{j=\tau_n}^{n} \Delta\varphi_j \approx 2^k \cdot \int d\varphi \; \forall t_n \,. \tag{8}$$

The counter value is loaded to an accumulator register every system clock cycle. The accumulator accumulates the counter value. The resulting accumulator register value is

$$\text{Accu}_{t_n} = \sum_{i=\tau_n}^{n} \text{Counter}_{t_i} \quad \forall t_n. \tag{9}$$

Insert (8) into (9)

$$\text{Accu}_{t_n} = \sum_{i=\tau_n}^{n} 2^k \cdot \sum_{j=\tau_i}^{i} \Delta\varphi_j = 2^k \cdot \sum_{i=\tau_n}^{n} \varphi_i \; \forall t_n \,. \tag{10}$$

Similar to (6) and (7)

$$\begin{aligned} \text{Accu}_{t_n} &= 2^k \cdot \sum_{i=\tau_n}^{n} \varphi_i \left[i - (i-1) \right] \\ &= 2^k \cdot \sum_{i=\tau_n}^{n} \varphi_i \cdot f_{sys} \cdot (t_i - t_{i-1}) \,. \end{aligned} \tag{11}$$

Therefore

$$\text{Accu}_{t_n} = 2^k \cdot 2^k \cdot \sum_{i=\tau_n}^{n} \varphi_i \cdot \Delta\varphi_i \approx 2^k \cdot 2^k \cdot \int \varphi d\varphi. \tag{12}$$

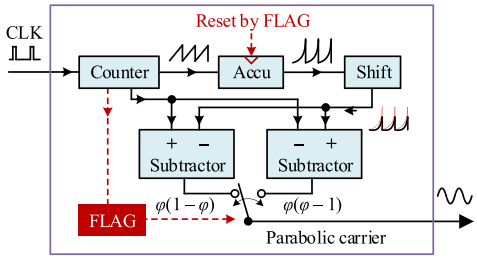

Fig. 4. Implementation of parabolic carrier.

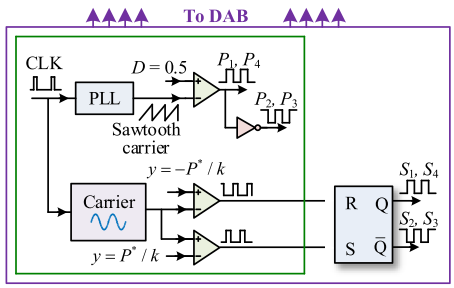

Fig. 5. Implementation of parabolic carrier and SR latch.

$y = \int 1 d\varphi - 2 \cdot \int \varphi d\varphi$ can be implemented as follows:

$$\text{Carrier} = 2^k \cdot \int d\varphi - 2^k \cdot 2 \cdot \int \varphi d\varphi = \text{Counter} - \text{Accu}/2^{k-1}. \tag{13}$$

The $\cdot/2^{k-1}$ operation can be implemented by a right shift of $k-1$ b. Therefore, the parabolic carrier can be implemented by

$$\text{Carrier} = \text{Counter} - (\text{Accu} \gg k-1) \,. \tag{14}$$

The implementation of $y = \varphi(\varphi - 1)$ is similar to $y = \varphi(1-\varphi)$ and, therefore, omitted in this letter. The implementation of parabolic carrier is shown in Fig. 4.

The counter-based PWM MCUs such as TI MCUs have already had a counter to generate the sawtooth or triangular carrier. If we can utilize the existing counter of this type of MCUs, only another three adders and a shifter are needed to realize the parabolic carrier. Please note that the cost of additional adders and shifters are extremely cheap for microcontroller manufacturing.

The carrier is then compared with reference $y = P^*/k$ and $y = -P^*/k$. The resulting pulses are given to a NOR/Positive NAND Gate SR latch to generate the gating signal. The implementation of parabolic carrier with SR latch is shown in Fig. 5. The resulting gating signal of Fig. 5 is presented in Fig. 3. The SR latch determines the rising edge and falling edge of the secondary side gating signal.

IV. Computation Time Assessment

The calculation of square root in DSP is time consuming. This results in poor computational efficiency. For example, it takes 63 CPU cycles for a 32-b fixed-point processor (TMS320F28035, etc.) to calculate a square root, whereas it takes around 6 CPU cycles to calculate a multiplication [10]. It takes 28 CPU cycles for a 32-b floating-point processor (TMS320F28335, etc.) to complete a square root calculation by using fast real-time support (RTS) library, whereas it takes one cycle to complete a

TABLE I
BENCHMARKS FOR EXECUTING TIME IN CPU CYCLES

	Floating point (Fast RTS)	IQMath	CLA (Floating point)
Summation	1*	1*	1*
Multiplication	1*	6*	1*
Division	24	63	13
Sine function	37	46	28
Square root	28	63	16

Unit: CPU cycles.
*Minimum cycles. Numbers may vary depending on compilers and arguments.

TABLE II
KEY PARAMETERS OF VERILOG

CPU frequency, f_{sys}	200 MHz
Switching frequency, f_{sw}	50 kHz
Frequency ratio, 2^k	2^{11}
Counter register	11 bits
Accumulator register	21 bits
Right shift	10 bits
Resolution	512

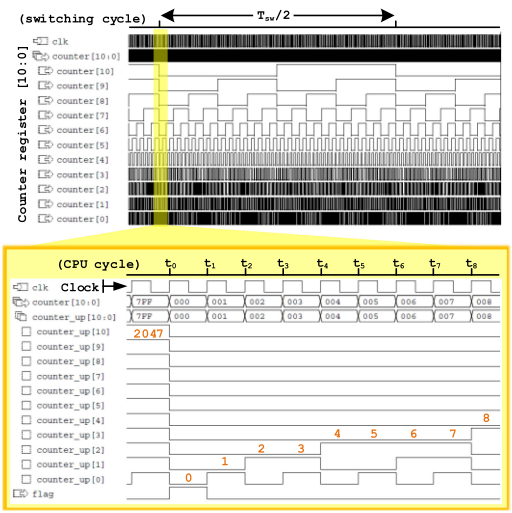

Fig. 6. Counter register result.

multiplication [2]. The Texas Instruments TMS320C28x series also provides a Control Law Accelerator (CLA) math library that optimizes the floating-point math functions. Table I summarizes the executing time of some frequently used operands. The calculation time of square root is generally 10–20 times longer than that of multiplication.

V. CASE STUDY

A. Parabolic Carrier

The proposed parabolic carrier is implemented in Verilog. The Verilog is simulated in Cadence/SimVision to visualize the outcome. The key parameters of Verilog implementation are summarized in Table II.

Figs. 6–8 show the Verilog visualized in Cadence/SimVision. Fig. 6 shows the counter register results. The counter adds one

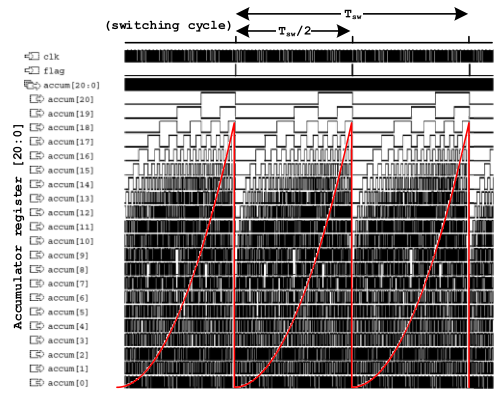

Fig. 7. Accumulator register result.

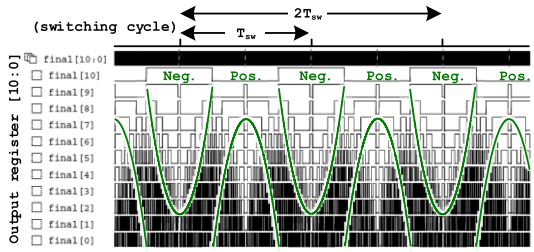

Fig. 8. Resulting parabolic output of Verilog script.

at every CPU cycle. The counter sets up a flag when the register is full (2047). The accumulator register result is shown in Fig. 7. Fig. 8 shows the parabolic carrier generated by the Verilog code. The maximum value is 512 which occupies a 10-b register to store. The 11th digit is a sign bit.

B. SRC Charging

The SRC charging has been discussed in [11]. The basic idea is charging the Li-ion battery with sinusoidal ripple current. The zero current zone of the SRC allows the ions in the battery electrolyte to be evenly distributed [12].

An electric vehicle (EV) on-board charger using SRC concept is studied as an example to present the advantage of the proposed modulation method. The circuit is called single-phase single-stage bidirectional DAB ac–dc converter [13], [14]. The key waveforms of the SRC-based EV on-board charger are shown in Fig. 9.

C. Computational Efficiency Assessment

In SRC charging, the charging power varies from zero to the peak value in every half fundamental cycle. Therefore, the square root value needs to be updated every switching cycle to achieve seamless transition. Assume half of the CPU resources are occupied by necessary system overhead. The remaining CPU resources are assigned to the converter control commands such as the over current/voltage protection, control algorithms, and phase shift update. The CPU resources in one switching cycle is a function of system clock and switching frequency

$$CC = f_{\mathrm{sys}}/\left(2f_{\mathrm{sw}}\right) \tag{15}$$

where CC is the number of CPU cycles in one switching cycle.

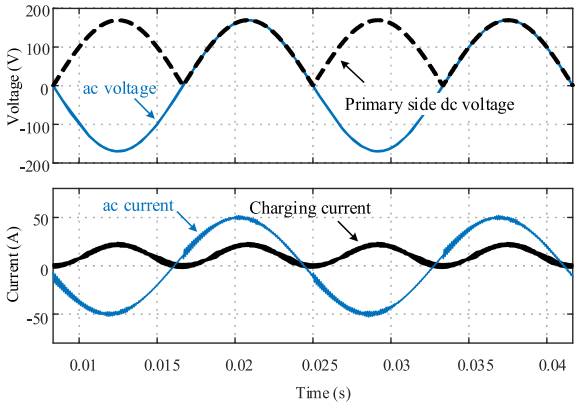

Fig. 9. Key waveforms of the SRC-based EV on-board charger.

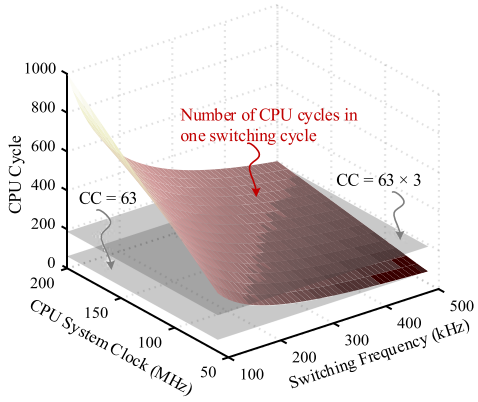

Fig. 10 Remaining CPU cycles in terms of system clock frequency and switching frequency.

Fig. 10 visualizes the CPU resources in terms of system clock frequency and switching frequency. If the proposed modulation method is adopted, the CPU resources under the grey plane can be saved. This becomes crucial in the high switching frequency area since the grey plane has exceeded CPU surface in this zone.

If the offline LUT is adopted, one LUT is needed for one operating point. For example, the SRC charging needs a table of 1667 entries if the switching frequency is 100 kHz and the fundamental frequency is 60 Hz. Note that this table is for one operating point only. If ten operating points are required, ten tables are needed. The missing operating points are calculated by interpolation. This will reduce the control accuracy. If the parabolic carrier is used instead, the LUTs and the interpolation calculation can be saved, as well as the control accuracy can be improved.

D. Feedback Control

In SRC charging, the charging power varies from zero to the peak power in every half fundamental cycle. The gain of the DAB transfer function varies from different power levels. If the wide range of power output is regulated by the feedback without an accurate feed forward loop, the controller will introduce harmonics into output power. This can be seen from the DAB modeling.

The circuit to conduct SRC charging is shown in Fig. 11. To simplify the analysis, $L_{\rm bat}$ is assumed to be small and the C_2 voltage is the same as the battery voltage. Therefore, V_{C2} is no longer a state variable. The high-frequency transformer model is replaced by the power transfer function

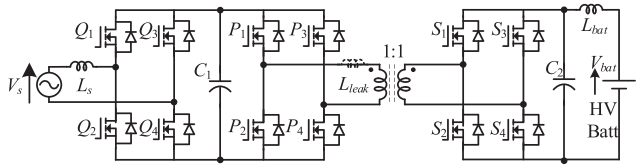

Fig. 11. The single-phase inverter interfaced DAB converter.

$$P = \frac{nV_{\rm C_1}V_{\rm C_2}}{2f_sL_{\rm leak}}\varphi\left(1-\varphi\right) \tag{16}$$

where $n = 1$ is the turns ratio of the transformer for this letter, f_s is the switching frequency, V_{C_1} and V_{C_2} are the capacitor voltages, and φ is the phase shift between primary voltage and secondary side voltage. The SPS control is adopted in this letter.

To find the gain of the phase shift to power transfer function, replace φ with $\tilde{\varphi}+\varphi_e$ and P with $\tilde{P}+P_e$. φ_e and P_e are the state variables at steady state

$$\tilde{P}+P_e = \frac{nV_{\rm C_1}V_{\rm C_2}}{2f_sL_{\rm leak}}\left(\tilde{\varphi}+\varphi_e-\left(\tilde{\varphi}+\varphi_e\right)^2\right). \tag{17}$$

Equation (17) can be simplified as

$$\tilde{P}+P_e = \frac{nV_{\rm C_1}V_{\rm C_2}}{2f_sL_{\rm leak}}\left(\tilde{\varphi}+\varphi_e-\tilde{\varphi}^2-{\varphi_e}^2-2\tilde{\varphi}\varphi_e\right). \tag{18}$$

Since the steady state has

$$P_e = \frac{nV_{\rm C_1}V_{\rm C_2}}{2f_sL_{\rm leak}}\left(\varphi_e-{\varphi_e}^2\right). \tag{19}$$

Therefore

$$\tilde{P} = \frac{nV_{\rm C_1}V_{\rm C_2}}{2f_sL_{\rm leak}}\left(\tilde{\varphi}-\tilde{\varphi}^2-2\tilde{\varphi}\varphi_e\right). \tag{20}$$

Omit the $\tilde{\varphi}^2$, the gain of $\tilde{\varphi}$ to $\tilde{P}$ is

$$\frac{\tilde{P}}{\tilde{\varphi}} = \frac{nV_{\rm C_1}V_{\rm C_2}}{2f_sL_{\rm leak}}\left(1-2\varphi_e\right). \tag{21}$$

As shown in (21), the gain of $\tilde{\varphi}$ to $\tilde{P}$ depends on the operating point. For example, when $P = 0$, which appears twice every fundamental cycle, the phase shift $\varphi_e = 0$. The transfer function gain is $\frac{nV_{\rm C_1}V_{\rm C_2}}{2f_sL_{\rm leak}}$. When $P = P_{\max}$, which is the peak value of every charging cycle, $\varphi_e = 0.5$. The gain of transfer function is zero. This means if a controller is designed with a constant gain, the error compensation capability of this controller varies at different power levels. If the SRC charging is executed solely depends on the feedback loop, the output power may have harmonic distortion.

If the proposed method is adopted, the parabolic carrier will automatically adjust the phase shift increment according to the operating point. For example, when $\varphi_e = 0$, the power reference makes a change of $\tilde{P}$. The phase shift will make a change of $\tilde{P}\cdot\frac{2f_sL_{\rm leak}}{nV_{\rm C_1}V_{\rm C_2}}$ because of the parabolic shape of the carrier. When $\varphi_e = 0.5$, the power reference makes a change of $\tilde{P}$ and the phase shift will become 1 because the reference has

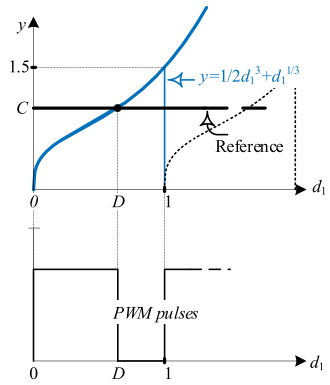

Fig. 12. Composite function carrier.

been above the carrier. This case can be deemed as the change of the phase shift is infinite. This infinite change is trying to match with the 0 gain at $\varphi_e = 0.5$. The role of the parabolic carrier is to force the DAB to follow the power reference. The gain of DAB to power can be deemed as a unity or a constant with parabolic carrier. Therefore, if a feedback controller is adopted together with the parabolic carrier, the error compensation capability of the controller is consistent in all power levels. Hence the controller will not introduce harmonic distortion to the output power.

E. Discussion

The concept of constructing PWM to simplify the duty cycle and/or phase shift can be extended to more complicated cases which even are deemed to be impractical to solve analytically. The proposed parabolic carrier demonstrates that the construction of PWM has the capability to graphically solve an equation. Any equation related to duty cycle or phase shift has the potential to use this capability of PWM pulses. The shape of the carrier may vary depending on the equation to solve. The parabolic carrier of this letter provides a simple method to eliminate the square root calculation. The power to phase shift calculation is selected as the key equation to simplify. Other equations such as the optimization objective functions, which is widely used in optimizing DAB operation, can also be selected as the key equation to simplify. Please note that the key equation must be a function of duty cycle or phase shift. The shape of the carrier does not necessarily be parabolic. For example, if the key equation is selected as follows:

$$\begin{cases} y = \frac{1}{2}{d_1}^3 + {d_1}^{1/3} \\ y = C. \end{cases} \tag{22}$$

Equation (22) has multiple solutions. The analytical solution of (22) cannot be easily derived with the aid of computer solver such as MATLAB or WolframAlpha. The numerical solution can be calculated when the coefficient is given under a specific case. Instead of solving (22) analytically, we can also solve it graphically by using nonlinear carrier. The carrier becomes a composite function, as shown in Fig. 12.

The intersection of the carrier and the reference is the solution of (22). This can greatly reduce the complexity of solving some complicated or high order equations. Although this letter focuses on the parabolic carrier, one can extend the similar idea to some even complicated cases.

VI. Conclusion

This letter proposed a simple phase-shift modulation using parabolic carrier for DAB dc–dc converters. The proposed method removes the square root computation from DAB control. This letter derives the parabolic carrier by releasing the constraint on carrier shape. The digital implementation of parabolic carrier concept is verified by Verilog. Compared with conventional online calculation method, the proposed method has the advantage in saving CPU computation resources. Compared with conventional LUT method, the proposed method saves CPU memory and improves the control accuracy. The proposed parabolic carrier based DAB is a good candidate for wide bandgap device (WBG) based DAB applications so that the converter can benefit most from the fast switching of WBG devices. Another advantage of the proposed method is its immunity to noise compared to the analog type of implementation. The proposed method is based on digital circuits, and digital circuits are generally considered to have higher noise immunity.

References

[1] B. Zhao, Q. Song, W. Liu, and Y. Sun, "Overview of dual-active-bridge isolated bidirectional DC-DC converter for high-frequency-link power-conversion system," *IEEE Trans. Power Electron.*, vol. 29, no. 8, pp. 4091–4106, Aug. 2014.

[2] "TMS320C28x floating point unit and instruction set reference guide," Texas Instrument-SPRUEO2B, 2015. [Online]. Available: http://www.ti.com/lit/ug/sprueo2b/sprueo2b.pdf

[3] F. Krismer and J. W. Kolar, "Closed form solution for minimum conduction loss modulation of DAB converters," *IEEE Trans. Power Electron.*, vol. 27, no. 1, pp. 174–188, Jan. 2012.

[4] K. M. Smedley and S. Cuk, "One-cycle control of switching converters," *IEEE Trans. Power Electron.*, vol. 10, no. 6, pp. 625–633, Nov. 1995.

[5] L. Zhang, "Derivation of parabolic current control with high precision, fast convergence and extended voltage control application," Ph.D. dissertation, Virginia Polytech. Inst. State Univ., 2016.

[6] L. Zhang *et al.*, "A dead-time compensation method for parabolic current control with improved current tracking and enhanced stability range," *IEEE Trans. Power Electron.*, vol. 30, no. 7, pp. 3892–3902, 2015.

[7] G. Wang and Y. W. Li, "Parabolic PWM for current control of voltage-source converters (VSCs)," *IEEE Trans. Ind. Electron.*, vol. 57, no. 10, pp. 3491–3496, 2010.

[8] Y. Liu, *et al.*, "Direct power control for dual active bridge converter with parabolic carrier," presented at the7th Workshop on Wide Bandgap Power Devices and Applications, Raleigh, NC, USA, 2019.

[9] C. Mi, H. Bai, C. Wang, and S. Gargies, "Operation, design and control of dual H-bridge-based isolated bidirectional DC–DC converter," *Int. Rev. Electr. Eng.*, vol. 6, no. 7, pp. 2846–2852, 2011.

[10] "C28x IQ math library," Texas Instrument, 2000. [Online]. Available: https://e2e.ti.com/cfs-file/__key/communityserver-discussions-components-files/171/C28x-IQmath-Library.pdf

[11] L. Chen, S. Wu, S. Member, D. Shieh, and T. Chen, "Sinusoidal-ripple-current charging strategy and optimal charging frequency study for Li-ion batteries," *IEEE Trans. Ind. Electron.*, vol. 60, no. 1, pp. 88–97, Jan. 2013.

[12] S. Cho, S. Member, and I. Lee, "Battery impedance analysis considering dc component in sinusoidal ripple-current charging," *IEEE Trans. Ind. Electron.*, vol. 63, no. 3, pp. 1561–1573, Mar. 2016.

[13] D. Sal, D. Frey, J. Schanen, and J. Ferrieux, "Isolated single stage bidirectional AC-DC converter with power decoupling and reactive power control to interface battery with the single phase grid," *IEEE Appl. Power Electron. Conf. Expo.*, pp. 631–636, 2018.

[14] J. Everts, F. Krismer, J. Van Den Keybus, J. Driesen, and J. W. Kolar, "Optimal ZVS modulation of single-phase single-stage bidirectional DAB AC-DC converters," *IEEE Trans. Power Electron.*, vol. 29, no. 8, pp. 3954–3970, Aug. 2014.